UWB Short-Range Bifocusing Tomographic Imaging

Lluís Jofre, *Senior Member, IEEE*, Anna Papió Toda, Josep Miquel Jornet Montana, Patricia Ceballos Carrascosa, Jordi Romeu, Sebastián Blanch, *Member, IEEE*, and Angel Cardama, *Member, IEEE*

***Abstract*—In this paper, the capability of ultra-wideband (UWB) sensor arrays for tomographic imaging of electrically large objects in 2-D and 3-D environments is presented. One of the main concerns when imaging extended real objects is the capability of the system to correctly reconstruct the object cross-section electric properties. An imaging method using a UWB multifrequency bifocusing (UWB-MFBF) operator with good tomographic imaging capabilities is presented, and numerical simulations are conducted to obtain the basic geometry and sampling parameters for a good-quality image reconstruction for geometrical and electrical parameters. Canonical-shape experimental reconstructions are performed to validate the established criteria.**

***Index Terms*—Antenna arrays, frequency domain, microwave imaging, near field, permittivity, tomography, ultra wideband (UWB).**

I. Introduction

THE CAPABILITY of microwave signals to penetrate and sense light opaque materials with reasonable spatial resolution makes them attractive for different industrial, medical, and security applications [1]–[5]. Wideband signals, such as those produced with ultra-wideband (UWB) systems [6], [7] and, in particular, the recent 3.1- to 10.6-GHz band, offer new possibilities to increase spatial resolution and material electrical parameter measurement accuracy.

Existing short-range imaging systems basically rely on two main techniques—the ones that are aimed at the internal inspection of the objects, normally based on tomographic approaches [8]–[13], and those that are based on the radar techniques [14]–[17], which are oriented at the characterization of specific scatters inside the interrogation zone. Although hybrid approaches exist, in general, radar-based techniques tend to be formulated in the time domain to use computationally efficient back-projection algorithms and to give accurate object shape and location results. Tomography-based techniques, on the other hand, tend to be formulated in the frequency domain to be based on nonlinear iterative inversion algorithms and to give accurate information on the dielectric-property profiles of the objects for modest size-contrast products. When the interest is the tomographic reconstruction of high-contrast electrically extended objects, the problem becomes highly nonlinear, and existing techniques suffer from a lack of accuracy (ill-conditioned matrices) or from low computational efficiency (time-expensive inversion or iterative methods); consequently, new approaches need to be found. Most of the imaging methods (both monofrequency and multifrequency) are frequency sensitive [18] in the sense that illuminating fields and their corresponding traces tend to be highly frequency dependent and, therefore, resonance modulated. On the other hand, a continuous frequency spectrum or, equivalently, a temporal impulse will reduce the resonance character of the reconstruction and, in some sense, the degree of nonlinearity.

The method presented in this paper, which theoretically completes and extends the previous work presented in [19], consists of a UWB multifrequency bifocusing (UWB-MFBF) imaging technique that synthetically focuses a UWB incident-transmitted field and the corresponding scattered-received field on every "pixel" of the reconstructed scenario. Using the wide frequency-band character of the incident-wave frequency, resonant-free reconstructions may be obtained. The establishment of criteria in terms of the number of sensors and their geometrical disposition will offer an interesting number of possibilities and improvements in the field of electromagnetic short-range object visualization.

In Section II, the analytical formulation is presented. In Section III, the spatial and frequency sampling criteria are established, and in Section IV, the quality of the reconstruction algorithm for low- and high-contrast objects is discussed. Parametric simulations have been conducted to verify the results.

A first experimental validation in Section V has been finally performed using two collinear arrays of UWB antennas, which act as transmitters and receivers.

II. Analytical Formulation

The general idea for UWB short-range imaging consists of distributing a certain number of microwave sensors (transmitters and/or receivers) on a certain region surrounding, as much as possible, the object under investigation. The goal is to obtain the 2-D or 3-D spatial and electrical information of the extended object, i.e., $\varepsilon_m(\vec{r})$, relative to the original background value of the interrogation area, i.e., $\varepsilon_b(\vec{r})$. The object can be a continuous distribution or a discrete set of independent objects S_k with electrical permittivity $\varepsilon_{S_k}(\vec{r})$.

Following the electromagnetic compensation principle [20], the illumination of an object induces an equivalent electric current distribution that is proportional to the electrical contrast

Manuscript received July 31, 2007; revised December 9, 2007. First published June 27, 2008; current version published October 10, 2008. This work was supported in part by the Spanish Centro de Investigación Científica y Tecnológica Project TEC2004-04866-C04-02 and Project TEC2007-66698-C04-01, in part by the European Commission under Contract EC-FP6-IST-508009 and under Contract EC-FP6-IST-026957, and in part by the Department of Universities, Generalitat de Catalunya, under SGR-00301. Portions of this paper have been reused, by permission, from the *Proceedings of the Third International Conference on Electromagnetic Near-Field Characterization and Imaging (ICONIC'07)*.

L. Jofre, A. Papió Toda, J. Romeu, S. Blanch, and A. Cardama are with the Polytechnic University of Catalonia, 08034 Barcelona, Spain.

J. M. Jornet Montana and P. Ceballos Carrascosa are with the Massachusetts Institute of Technology, Cambridge, MA 02139-4307 USA.

Color versions of one or more of the figures in this paper are available online at http://ieeexplore.ieee.org.

Digital Object Identifier 10.1109/TIM.2008.926382

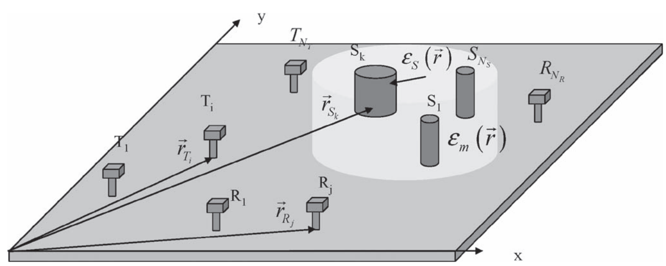

Fig. 1. Interrogation geometry.

$c(\vec{r}) = (\varepsilon_m(\vec{r}) - \varepsilon_b(\vec{r}))/\varepsilon_b(\vec{r})$ that, in the illumination process, may be seen as the source of the scattered field and, in the inverse imaging process, as an approximate "trace" of the original object.

As shown in Fig. 1, a set of N_T transmitters T_i and a set of N_R receivers R_j are used to scan the interrogation area where the reconstruction algorithm is applied. First, a measurement matrix (information matrix) is obtained as follows. For every transmitting element, the receiving array is scanned over each receiving element, obtaining an N_R measurement vector. Then, the procedure is repeated for the N_T transmitting elements, obtaining an $N_T \times N_R$ matrix.

The reconstruction algorithm forms every image point of the local electrical properties of the object by means of synthesizing two focused groups of antennas (transmitters and receivers). The antenna elements (transmitting and receiving signals) are numerically weighted by a focusing operator to be focused on a unique object point. This is achieved by a mathematical treatment of the measurement matrix. This numerical focusing operator [21] consists of taking the inverse weights of the electrical field that is induced by an imaginary object point that scans all the possible grid points of the space under reconstruction. Applying this focusing operator to the measurement matrix for all the points of the image space grid, we are able to obtain a replica of the extended object. Since there exist nonlinear phenomena, such as multiple or high-contrast scattering and frequency dependence, the continuous frequency superposition that is proposed in this paper will tend to smooth out and reduce their effects.

To be more specific, in the 2-D case, for a particular wavenumber k corresponding to the frequency f, the scattered field that is measured at a receiver positioned in $r_R(x_r, y_r)$ having an imaginary pointlike scatter placed at $r_S(x_s, y_s)$ is given by

$$E_s(x_r, y_r, f) = E_i(x_s, y_s, f) \cdot I_{\text{obj}} \cdot H_0^{(2)}(k|r_r - r_s|) \quad (1)$$

where H_0^2 is the Hankel function of the first order and the second kind, $I_{\text{obj}}(\vec{r}) \propto f c(\vec{r})\, E_i(\vec{r})$ [9] is the equivalent current induced on the object, and E_i is the focused incident field on the pointlike scatter position. This incident field can be expressed as

$$E_i(x_i, y_i, f) = \sum_{n=1}^{N_t} I_{tn}(x_f, y_f, f) \cdot H_0^{(2)}(k|r_{tn} - r_i|) \quad (2)$$

$$I_{tn}(x_f, y_f, f) = \frac{1}{H_0^{(2)}(k|r_{tn} - r_f|)} \quad (3)$$

where I_{tn} is the focusing operator for the transmitters.

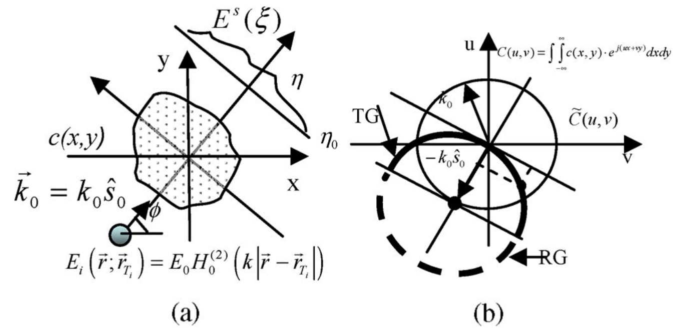

Fig. 2. (a) Space and (b) spectral domain geometry.

Then, the reconstructed field E_f in each of the focusing points of the grid is found as follows:

$$E_f(x_f, y_f, f) = \sum_{n=1}^{N_{rt}} I_{rn}(x_f, y_f, f) \cdot E_s(x_{rn}, y_{rn}, f) \quad (4)$$

$$I_{rn}(x_f, y_f, f) = \frac{1}{H_0^{(2)}(k|r_{rn} - r_f|)} \quad (5)$$

where I_{rn} is the focusing operator for the receivers.

Last, the entire process can be grouped using a matrix formulation as follows:

$$E_f(x_f, y_f) = [I_{t_1} \;\; I_{t_2} \;\; I_{t_3} \;\; \cdots \;\; I_{t_{N_t}}] \cdot \begin{bmatrix} E_{st_1r_1} & E_{st_1r_2} & \cdots & \cdots & E_{st_1r_{N_r}} \\ E_{st_2r_1} & \ddots & & & \vdots \\ E_{st_2r_1} & & \ddots & & \vdots \\ \vdots & & & \ddots & \vdots \\ E_{st_{N_t}r_1} & \cdots & \cdots & \cdots & E_{st_{N_t}r_{N_r}} \end{bmatrix} \cdot \begin{bmatrix} I_{r_1} \\ I_{r_2} \\ I_{r_3} \\ \vdots \\ I_{r_{N_r}} \end{bmatrix}. \quad (6)$$

For the UWB case, when a certain set of frequencies are combined, the total field can be obtained as a coherent addition, i.e.,

$$E_f(x_f, y_f) = \sum_{f=f_1}^{f_2} E_f(x_f, y_f, f). \quad (7)$$

The extension to the 3-D geometry can be done using the 3-D spherical operator e^{-jkr}/r instead of the 2-D Hankel operator.

III. SPACE AND FREQUENCY SAMPLING CRITERIA

Our aim is to obtain accurate spatial information about the electrically extended object in terms of its geometrical shape and electrical parameter values using a network of antennas that are located regularly or randomly throughout the interrogation area. The knowledge of the number of elements that must form the sensor network and its disposition on the reconstructing scenario is crucial to obtain the desired results.

Based on the Fourier diffraction theorem [22], the imaging problem can be stated as follows. The information obtained from the scattered field E^s produced by a particular frequency f_0 and orientation ϕ_0 [Fig. 2(a)] may be translated into a

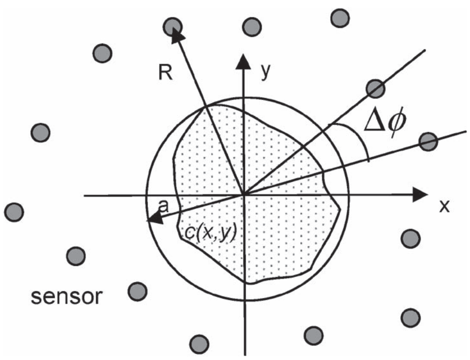

Fig. 3. Imaging sensor network geometry.

circle of radius $k_0 = 2\pi f_0 \sqrt{\mu_b \varepsilon_b}$ (semicircle TG for transmitting geometry and semicircle RG for reflection geometry) of the 2-D Fourier transform (FT) spectral domain (u, v) of the object $C(u, v) = \mathrm{FT}\{c(x, y)\}$ [Fig. 2(b)]. The successive angular and frequency scans will fill the spectral domain "knowledge" on a specific manner, depending on the imaging system design.

Under the low-contrast electrical property condition, i.e., $c(\vec{r}) \ll 1$, which is usually known as the Born condition, frequency and geometrical scans are partially equivalent, and optimized combinations can be found to fulfil the spectral domain C. Under the non-Born condition, however, those conditions are not applicable, and new criteria need to be obtained.

To design the UWB imaging system, the spatial and frequency requirements need to be considered, according to the following points.

1) Spatial-Angular Sampling: From the electromagnetic modal expansion of the fields scattered by an electric object when illuminated by an incident field, it is known that to obtain an image with a resolution of $\lambda_{f_{\max}}/2$ (with $\lambda_{f_{\max}}$ being the highest operating frequency inside the UWB interval), in all directions, good encircling interrogation geometry with a number N_ϕ of views is required. The minimum number of views that are necessary to properly reconstruct the object is equal to the number of coefficients of the cylindrical-mode (or the spherical mode for 3-D geometry) expansion [20] of the scattered field, i.e.,

$$N_\phi \geq 2k_{f_{\max}} a = 2 \cdot \pi \cdot a/(\lambda_{f_{\max}}/2) \tag{8}$$

with a being the object-encircling radius, and $k_{f_{\max}} = 2\pi/\lambda_{f_{\max}}$.

Thus, implying a maximum angular step, as shown in Fig. 3

$$\Delta\phi = 2 \cdot \pi/N_\phi = \lambda_{f_{\max}}/(2 \cdot a). \tag{9}$$

Fig. 4 shows the reconstruction results for a dielectric cylinder with a diameter of 25 cm using encircling circular geometry with 128 transceivers [sequentially acting as emitters and receivers; Fig. 4(a)] and 16 transceivers [Fig. 4(b)]. When angular sampling criteria are satisfied [$N_\phi > 2ka$; Fig. 4(a)], the reconstructed image is uniform over the cylinder, and the contours are determined perfectly.

2) Frequency Sampling: To ensure an image that is free of distortion and false aliases into the radial (Fig. 3) direction,

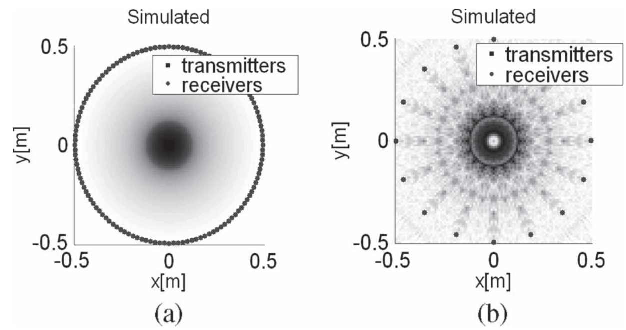

Fig. 4. Reconstructed image of a 25-cm diameter cylinder with (a) 128 emitters and receivers and (b) 16 emitters and receivers.

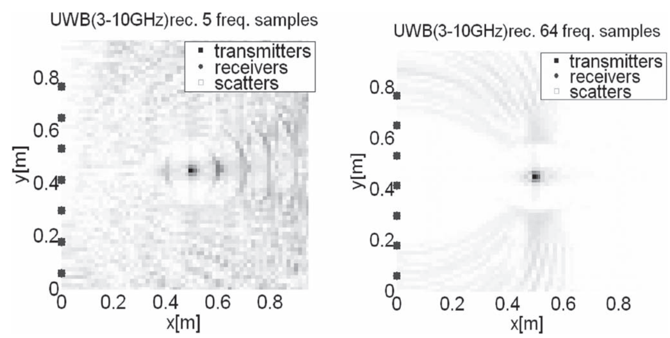

Fig. 5. Object aliases versus the number of frequency samples.

the frequency sampling Δf must accomplish the following (for $R_{\min} = 2a$):

$$\Delta f \leq \frac{1}{T_t} = \frac{c}{2R_{\min}} = \frac{c}{4a}. \tag{10}$$

Therefore, given a certain frequency bandwidth of $B = f_{\max} - f_{\min}$, which is associated with a pulse of spatial length l_p, the number of frequency samples N_f to obtain an image of the extended object without replicas inside the area of interest must be

$$N_f \geq \frac{f_{\max} - f_{\min}}{\frac{c}{2R}} = \frac{B}{\frac{c}{2R}} = \frac{2a}{l_p}. \tag{11}$$

Fig. 5(a) has been obtained with fewer samples $(N_f = 5)$ than that given by (2) with $R = 1$ m. Distorted aliases appear every 10 cm. Fig. 5(b), on the other hand, has been obtained with an appropriate number of frequencies $(N_f = 64)$; therefore, the replicas are out of range.

3) Measurement Geometry: Last, the measurement arrangement needs to be considered. For reflection geometry [Fig. 6(a)], only the contours of the cylinder in the direction that is orthogonal to the array are well defined, and there is not much information on the internal profile of the object. By increasing the number of views, the whole contour would be determined. On the other hand, for transmission geometry [Fig. 6(b)], the edges tend to disappear, and the internal characteristics of the object are reinforced.

When using circular geometry [Fig. 6(c)], where all antennas are transmitters and receivers at the same time, a high-quality image of the whole object is obtained. In accordance with the aforementioned Fourier diffraction theorem [22], the observed differences between the reconstructed images corresponding to

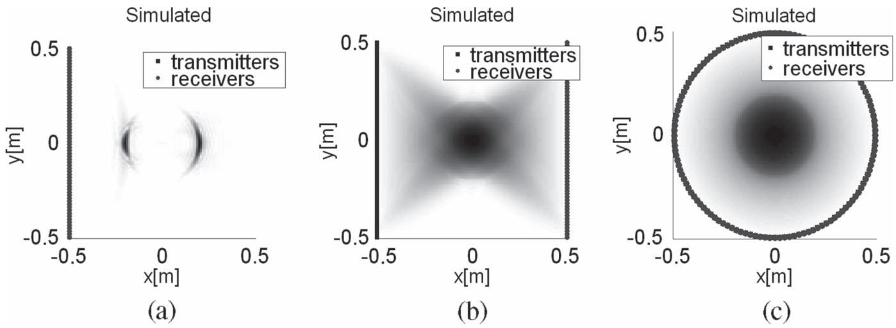

Fig. 6. Reconstructed cylinder of radius 0.2 m and $\varepsilon_d = 1.01$. (a) Reflection geometry. (b) Transmission geometry. (c) Circular geometry.

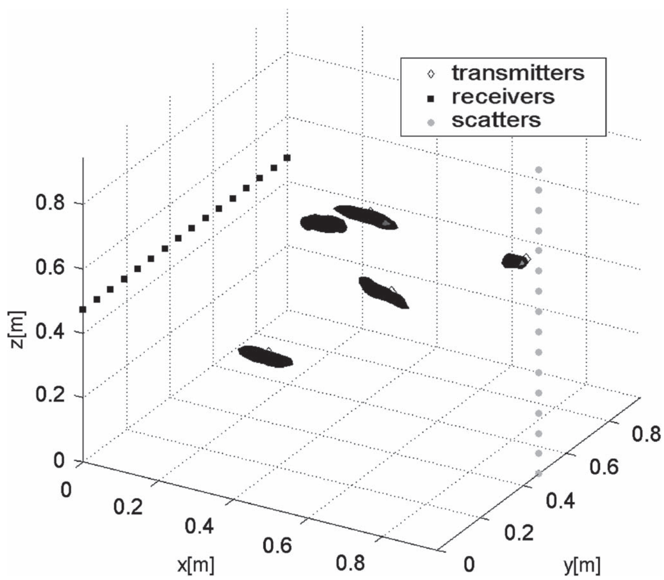

Fig. 7. Three-dimensional reconstructed image for a UWB Mills crossed linear array.

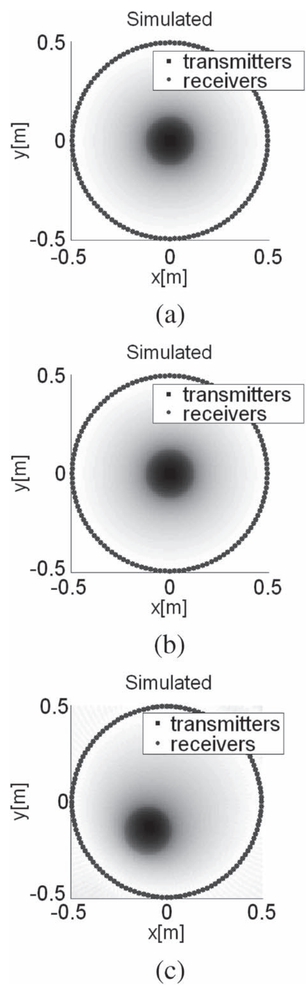

Fig. 8. Reconstructed cylinder with a diameter of 0.25 m, and $\varepsilon_d = 1.01$. (a) At 10.6 GHz. (b) Using the whole UWB 3.1–10.6 GHz. (c) Off-centered cylinder using the whole UWB frequency range.

the previous three kinds of antenna geometry are related to the way the spectral domain has been filled with the different measurement arrangements.

For nonencircling geometry, such as the linear geometry shown in Fig. 6(a) and (b), the resolution decreases in the transversal axis due to the lack of information on the associated area of the spectral domain. In this case, the transversal resolution, instead of being close to $\lambda_{f_{\max}}/2$, is $R\lambda_{f\,\max}/L_{\text{array}}$, where L_{array} is the length of the antenna array, and R is the distance from the object to the sensor antennas.

Last, when the interest is on 3-D geometry, appropriate sensor geometry has to be considered. The Mills cross array [23] is a good resolution array complexity tradeoff. Fig. 7 shows the reconstructed image for a set of five spherical 6-cm diameter objects inside $100 \times 100 \times 100$ cm^3 when sensed by two 100-cm-length linear arrays—a horizontal array of transmitters and a vertical array of receivers.

IV. Image Reconstruction Quality

In this section, the quality of the image for different values of the electrical contrast for a UWB sensor network that accomplishes the previous sampling criteria is tested, and basic guidelines for good image reconstruction quality are obtained.

1) Born Object Imaging: Under low-contrast Born objects, frequency and spatial scanning are partially equivalent (giving almost equivalent information), and optimized combinations of the previous equations can be found to fill the spectral domain and to obtain the correct image of the object. Fig. 8(a) shows how the monofrequency image obtains a good reconstruction of the electrical contrast that is equivalent to the one obtained with the whole UWB frequency range [Fig. 8(b)]. Fig. 8(c) shows the equivalent results for an off-centered cylinder. In this low-contrast case, a single frequency and a dense angular sampling may be equivalent to a dense frequency sampling combined with a reduced number of views.

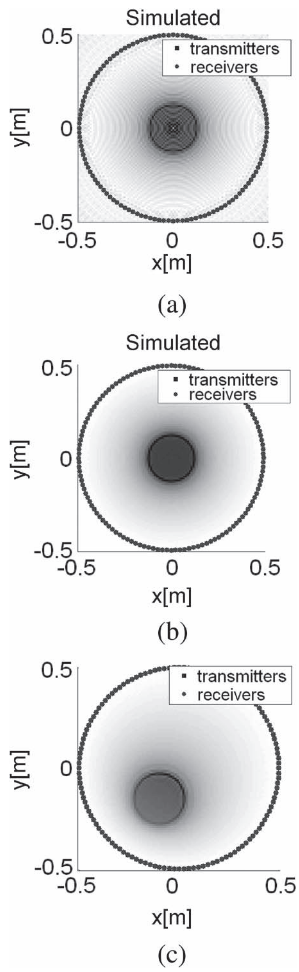

Fig. 9. Reconstructed cylinder with a diameter of 0.25 m, and $\varepsilon_d = 100$. (a) At 10.6 GHz. (b) Using the whole UWB 3.1–10.6 GHz. (c) Off-the-center-positioned cylinder using the whole UWB frequency range.

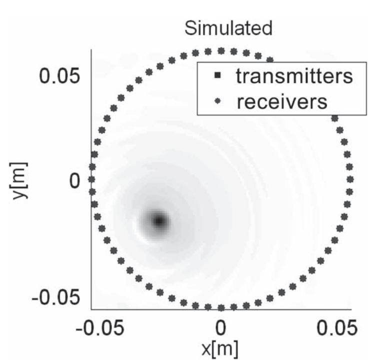

Fig. 10. Tumor detection in a medium with $\varepsilon_m = 7 - 0.3j$. Tumor radius is 2.5 mm, and $\varepsilon_s = 50$.

2) Non-Born Object Imaging: Under non-Born conditions, UWB proves to succeed in obtaining high-quality images, whereas it is not possible using a single frequency. Fig. 9 shows, for high contrasted objects, how the frequency scan [see Fig. 9(b)] improves the quality of the monofrequency reconstruction [see Fig. 9(b)]. Fig. 9(c) shows how the quality of the reconstruction can be maintained for an off-centered cylinder.

Object Imaging in "Permeable" Media: One of the quality parameters of an imaging system is its capability to reconstruct objects that are immersed in real "permeable" backgrounds. As one of the cases of growing interest is cancer detection, we present the imaging results for a simple model of a breast tumor using the UWB-MFBF method. Fig. 10 shows how the tumor can be properly reconstructed in spite of being inside a fat lossy layer.

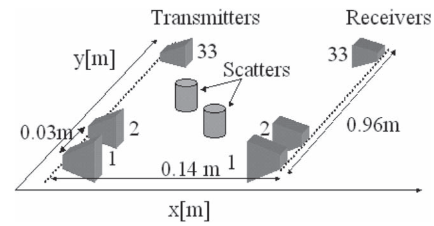

Fig. 11. Geometry of the location experimental setup.

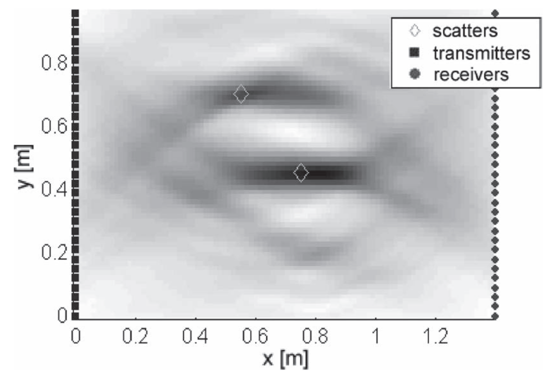

Fig. 12. Experimental reconstruction of the two scatters using the UWB-MFBF method.

V. Experimental Results

To perform some preliminary validation of the previous imaging results, experimental UWB measurements (3.1–10.6 GHz) were done. Measurements were taken inside an anechoic chamber to avoid excessive reflections from the environment.

As a first canonical case, two cylindrical scatters with a diameter of 6 cm $(2\lambda_{f_{\max}})$ were placed inside a 96 × 140 cm rectangular interrogation area formed by two robotized linear scanning systems, as shown in Fig. 11. Two UWB ridge antennas, respectively acting as a transmitter, and a receiver, were connected to a 40-GHz Agilent vector network analyzer and moved along the 96-cm scanning systems in steps of 3 cm, forming a 33 × 33 element measurement matrix (for each of the 33 positions of the transmitting antenna, 33 measurements corresponding to the 33 receiving antenna positions were recorded).

Fig. 12 presents the results for the two canonical 6-cm diameter cylindrical objects using the UWB-MFBF technique, showing that the cylinders are correctly placed with a $\lambda_{f_{\max}}/2$ resolution along the y-axis but are poorly placed along the longitudinal z-axis due to the lack of the encircling characteristic of the sensors.

For a more realistic situation, a cylinder with a diameter of 30 cm $(10\lambda_{f_{\max}})$ filled with water was placed between the two synthetic linear arrays that were described previously. Results for the reconstruction (Fig. 13) show the correct placement of the cylinder, a quite uniform reconstruction of the inside,

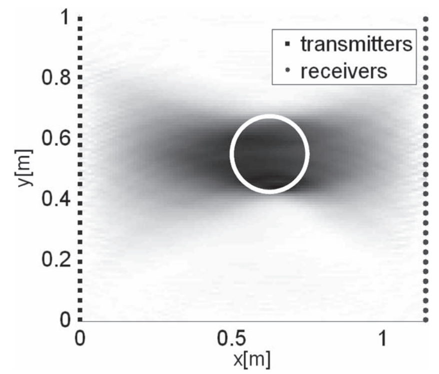

Fig. 13. Experimental reconstruction of a cylinder of water and 0.3-m diameter using the UWB-MFBF imaging method.

and good contour accuracy on the y-axis and poorer accuracy in the x-axis, again, because not enough encircling geometry was used.

VI. Conclusion

UWB characteristics give a set of unique possibilities in terms of resolution and robustness for the tomographic visualization capabilities of arbitrary interrogation geometry. The resolution can reach $\lambda/2$, at the highest operating frequency, in all directions for circular or random geometry. For 3-D interrogation geometry, the crossed linear geometry can be made appropriate when a reduction on the number of sensors is necessary.

UWB short-range imaging is possible for Born and non-Born objects under certain sampling criteria for frequency and spatial scanning.

For low-contrast Born objects, optimization on the established criteria can be applied, as frequency and geometrical data are partially equivalent.

For high-contrast objects, simultaneous accomplishment of the two sampling criteria (the frequency and the angle) gives better reconstructed images due to the nonresonant characteristic of the UWB illuminating field.

References

[1] R. Zoughi, *Microwave Testing and Evaluation*. Amsterdam, The Netherlands: Kluwer, 2000.

[2] J. C. Bolomey, *Frontiers in Industrial Process Tomography*. London, U.K.: Eng. Foundation, 1995.

[3] L. E. Larsen and J. H. Jacobi, Eds., *Medical Applications of Microwave Imaging*. Piscataway, NJ: IEEE Press, 1986.

[4] E. C. Fear, P. M. Meaney, and M. A. Stuchly, "Microwaves for breast cancer detection," *IEEE Potentials*, vol. 22, no. 1, pp. 12–18, Feb./Mar. 2003.

[5] M. Pastorino, "Short-range microwave inverse scattering techniques for image reconstruction and applications," *IEEE Trans. Instrum. Meas.*, vol. 47, no. 6, pp. 1419–1427, Dec. 1998.

[6] J. D. Taylor, Ed., *Introduction to Ultra-Wideband Radar Systems*. Boca Raton, FL: CRC, 1995.

[7] R. Zetik, J. Sachs, and R. S. Thoma, "UWB short-range radar sensing," *IEEE Instrum. Meas. Mag.*, vol. 10, no. 2, pp. 39–45, Apr. 2007.

[8] M. Benedetti, M. Donelli, A. Martini, M. Pastorino, A. Rosani, and A. Massa, "An innovative microwave-imaging technique for nondestructive evaluation: Applications to civil structures monitoring and biological bodies inspection," *IEEE Trans. Instrum. Meas.*, vol. 55, no. 6, pp. 1878–1884, Dec. 2006.

[9] A. Broquetas, J. Romeu, J. M. Rius, A. Elias, A. Cardama, and L. Jofre, "Cylindrical geometry: A further step in active microwave tomography," *IEEE Trans. Microw. Theory Tech.*, vol. 39, no. 5, pp. 836–844, May 1991.

[10] A. Joisel, J. Mallorqui, A. Broquetas, J. M. Geffrin, N. Joachimowicz, M. V. Lossera, L. Joire, and J. C. Bolomey, "Microwave imaging techniques for biomedical applications," in *Proc. 16th IEEE IMTC*, May 24–26, 1999, vol. 3, pp. 1591–1596.

[11] T. C. Guo and W. W. Guo, "High resolution microwave imaging simulation of human neck," in *Proc. 16th IEEE IMTC*, May 24–26, 1999, vol. 3, pp. 1586–1590.

[12] S. Y. Semenov, A. E. Bulyshev, A. Abubakar, V. G. Posukh, Y. E. Sizov, A. E. Souvorov, P. M. van den Berg, and T. C. Williams, "Microwave-tomographic imaging of the high dielectric-contrast objects using different image-reconstruction approaches," *IEEE Trans. Microw. Theory Tech.*, vol. 53, no. 7, pp. 2284–2294, Jul. 2005.

[13] N. N. Qaddoumi, M. Abou-Khousa, and W. M. Saleh, "Near-field microwave imaging utilizing tapered rectangular waveguides," *IEEE Trans. Instrum. Meas.*, vol. 55, no. 6, pp. 1752–1756, Oct. 2006.

[14] J. Modelski, M. Bury, and Y. Yashchyshyn, "Short-pulse microwave imaging system," in *Proc. 5th Int. Conf. MEMIA*, Dec. 13–15, 2005, pp. 31–36.

[15] E. C. Fear, X. Li, S. C. Hagness, and M. A. Stuchly, "Confocal microwave imaging for breast cancer detection: Localization of tumors in three dimensions," *IEEE Trans. Biomed. Eng.*, vol. 49, no. 8, pp. 812–822, Aug. 2002.

[16] E. J. Bond, L. Xu, S. C. Hagness, and B. D. Van Veen, "Microwave imaging via space-time beamforming for early detection of breast cancer," *IEEE Trans. Antennas Propag.*, vol. 51, no. 8, pp. 1690–1705, Aug. 2003.

[17] F. -C. Chen and C. Chew, "Time-domain ultra-wideband microwave imaging radar system," in *Proc. 15th IEEE IMTC*, May 18–21, 1998, vol. 1, pp. 648–650.

[18] A. Fhager, P. Hashemzadeh, and M. Persson, "Reconstruction quality and spectral content of an electromagnetic time-domain inversion algorithm," *IEEE Trans. Biomed. Eng.*, vol. 53, no. 8, pp. 1594–1604, Aug. 2006.

[19] A. Papió, J. M. Jornet, P. Ceballos, J. Romeu, S. Blanch, A. Cardama, and L. Jofre, "UWB short range imaging," presented at the Third Int. Conf. Electromagn. Near-Field Characterization Imaging, St. Louis, MO, 2007.

[20] R. F. Harrington, *Time-Harmonic Electromagnetic Fields*. New York: McGraw-Hill, 1961.

[21] Y. J. Kim, L. Jofre, F. De Flaviis, and M. Q. Feng, "Microwave reflection tomographic array for damage detection of civil structures," *IEEE Trans. Antennas Propag.*, vol. 51, no. 11, pp. 3022–3032, Nov. 2003.

[22] M. Slaney and A. C. Kak, "Limitations of imaging with first-order diffraction tomography," *IEEE Trans. Microw. Theory Tech.*, vol. MTT-32, no. 8, pp. 860–874, Aug. 1984.

[23] J. M. Girones, L. Jofre, M. Ferrando, E. Reyes, and J. C. Bolomey, "Microwave imaging with crossed linear arrays," *Proc. Inst. Electr. Eng.–H*, vol. 134, no. 3, pp. 249–252, Jun. 1987.

Lluís Jofre (S'79–M'83–SM'07) was born in Mataró, Spain, in 1956. He received the M.Sc. (Ing.) and Ph.D. (Dr.Ing.) degrees in electrical engineering (telecommunications engineering) from the Polytechnic University of Catalonia (UPC), Barcelona, Spain, in 1978 and 1982, respectively.

From 1979 to 1980, he was a Research Assistant with the Electrophysics Group, UPC, where he worked on the analysis and near-field measurement of antenna and scatterers. From 1981 to 1982, he was with the Ecole Superieure d'Electricite, Paris, France, where he was involved in microwave antenna design and imaging techniques for medical and industrial applications. In 1982, he was an Associate Professor with the Department of Communications, Telecommunication Engineering School, UPC, where he became a Full Professor in 1989. From 1986 to 1987, he was a Visiting Fulbright Scholar with Georgia Institute of Technology, Atlanta, where he worked on antennas and electromagnetic imaging and visualization. From 1989 to 1994, he served as the Director of the Telecommunication Engineering School, UPC. From 1994 to 2000, he was the Vice Rector for Academic Planning at UPC. From 2000 to 2001, he was a Visiting Professor with the Department of Electrical and Computer Engineering, Henry Samueli School of Engineering, University of California, Irvine. From 2002 to 2004, he was the Director of the Catalan Research Foundation. Since 2003, he has been the Director of the UPC Telefónica Chair. He has authored more than 100 scientific and technical papers, reports, and chapters in specialized volumes. His research interests include antennas, electromagnetic scattering and imaging, and system miniaturization for wireless and sensing industrial applications and bioapplications.

Anna Papió Toda was born in Reus, Spain, in 1984. She is currently working toward the M.S. degree in telecommunication engineering studies and computer sciences at the Polytechnic University of Catalonia (UPC), Barcelona, Spain.

Since February 2006, she has been a Research Assistant with the Department of Signal Theory and Communications, UPC, where she is working on UWB imaging and location systems. During July–August 2006, she was a Visiting Researcher with the Institut für Höchstfrequenztechnik und Elektronik, Universität Karlsruhe, Karlsruhe, Germany, where she worked on UWB antenna characterization by means of FDTD simulations. Her research interests include antennas, electromagnetic scattering and imaging, and wireless systems.

Josep Miquel Jornet Montana was born in Tarragona, Spain, in 1984. He is currently working toward the M.S. degree in telecommunication engineering studies and the M.S. degree in information and communication technologies at the Polytechnic University of Catalonia (UPC), Barcelona, Spain.

From February 2006 to July 2007, he was a Research Assistant with the Department of Signal Theory and Communications, UPC, where he worked on UWB imaging and location systems. He is currently a Visiting Researcher with the Massachusetts Institute of Technology, Cambridge, where he is working on the design of routing protocols for underwater acoustic networks. His research interests include antennas, electromagnetic scattering and imaging, wireless systems, and sensor networking.

Patricia Ceballos Carrascosa was born in Logroño, Spain, in 1984. She is currently working toward the M.S. degree in telecommunication engineering studies and the M.S. degree in information and communication technologies at the Polytechnic University of Catalonia (UPC), Barcelona, Spain.

From February 2006 to July 2007, she was a Research Assistant with the Department of Signal Theory and Communications, UPC, where she worked on UWB imaging and location systems. She is currently a Visiting Researcher with the Massachusetts Institute of Technology, Cambridge, where she is working on signal processing for underwater communications. Her research interests include antennas, electromagnetic scattering and imaging, wireless systems, and signal processing.

Jordi Romeu was born in Barcelona, Spain, in 1962. He received the B.S. and Ph.D. degrees in Ingeniero de Telecomunicación from the Universitat Politècnica de Catalunya (UPC), Barcelona, in 1986 and 1991, respectively.

Since 1985, he has been with the Photonic and Electromagnetic Engineering Group, Department of Signal Theory and Communications, UPC, where he is currently a Full Professor, engaged in research on antenna near-field measurements, antenna diagnostics, and antenna design. In 1999, he was a Visiting Scholar with the Antenna Laboratory, University of California, Los Angeles, on a North Atlantic Treaty Organization Scientific Program Scholarship and, in 2004, with the University of California, Irvine. He is the holder of several patents and has authored 35 refereed papers in international journals and 50 conference proceedings.

Dr. Romeu was the grand winner of the 1998 European IT Prize, which was awarded by the European Commission, for his contributions to the development of fractal antennas.

Sebastián Blanch (M'91) was born in Barcelona, Spain, in 1961. He received the Sc.M. and Ph.D. degrees in telecommunication engineering from the Polytechnic University of Catalonia (UPC), Barcelona, in 1989 and 1996, respectively.

Since 1989, he has been with the Electromagnetic and Photonics Engineering Group, Department of Signal Theory and Communications, UPC, where he is currently an Associate Professor. His research interests include near-field antenna measurements and imaging, antenna diagnostics, and antenna design.

Angel Cardama (S'67–M'73) was born in Santiago de Compostela, Spain, in 1944. He received the Ingeniero de Telecomunicación degree from the Universidad Politécnica de Madrid, Madrid, Spain, in 1968 and the Sc.M. and Ph.D. degrees in electrical engineering from Brown University, Providence, RI, in 1970 and 1973, respectively.

Since 1972, he has been with the faculty of the Telecommunication Engineering School, Polytechnic University of Catalonia, Barcelona, Spain, where he is currently a Professor. His research interests range from the development of analytical and numerical techniques in electromagnetics to the design of microwave imaging systems and radar and communication antennas.